Synthesis and characterization of Fe-doped CuO nanoparticles: Catalytic efficiency in crystal violet dye degradation and exploration of electrical properties

Bushra[1], Muhammad Kashif[1], Khairullah[1], Azmat Ali Khan[1], Hao Sun[2,3], Jasim Yousaf[4], Muhammad Ishaq Ali Shah[1], Shah Hussain[5], Jalal Amir[4], Yousaf Jamal[1] & Taimoor Ahmad[1]

[1] Department of Chemistry, Abdul Wali Khan University Mardan, Mardan-23200, Pakistan

[2] Faculty of Science, Autonomous University of Madrid, Madrid-28049, Spain

[3] Cantoblanco Campus, Consejo Superior de Investigaciones Cientificas, CSIC, Madrid-28049, Spain

[4] Department of Physics, Abdul Wali Khan University Mardan, Mardan-23200, Pakistan

[5] Government Postgraduate College Nowshera, Nowshera-24100, Pakistan

Corresponding Author: Muhammad Kashif, Department of Chemistry, Abdul Wali Khan University Mardan, Mardan-23200, Pakistan. E-mail: mkashifsgr1@gmail.com

Received: May 01, 2024 DOI: 10.14295/bjs.v3i8.601

Accepted: June 13, 2024 URL: https://doi.org/10.14295/bjs.v3i8.601

Abstract

In recent times, environmental pollution has become a pressing issue. Different methods have been developed to detach hazardous materials from H_2O bodies. Among these techniques, photo-catalysis has emerged as a low-cost and advanced method. However, finding a potent photocatalyst has been a topic of considerable research. Our study prepared CuO from copper acetate using hydrothermal treatment in an autoclave at 170 ºC for 14 hours. We introduced various quantities of Fe by adding FeSO4 mixture to Cu $(CH_3COO)_2$, following the identical method for preparing CuO. The resulting precipitate was cleaned with deionized H_2O and dried at 100 °C. The prepared substance was then heated at 450 ºC in a muffle furnace for 60 minutes. We characterized the manufacture of photocatalysts utilizing various techniques such as Ultraviolet (UV), FT-IR, SEM, EDX, and XRD. Our Ultraviolet (UV) spectrum analysis helped us recognize the adsorption spectroscopic analysis of un-doped and doped CuO with various ratios of Fe. FTIR spectroscopic analysis helped us identify functional groups in CuO NPs. Our XRD study showed the monoclinic composition of copper oxide nanoparticles. The SEM picture suggested that NPs exist in a spherical shape. We studied the catalytic activity of synthesized NPs concerning crystal violet (CV) colorant degradation below a direct ray of light irradiation. Our results showed that the degradation productiveness, as compared to CV colorant, was about 93.52% in 180 min. This research is of great importance in the quest for effective and sustainable solutions to environmental problems. The examination of electrical properties highlighted the promising aspects of Fe-doped CuO, particularly at 6% doping. This variant demonstrated superior dielectric parameters, lower tangent loss, semiconductor-like impedance behavior, and enhanced electrical conductivity, emphasizing its potential for applications in electrical and energy storage domains.

Keywords: hydrothermal method, photocatalytic degradation, crystal violet dye.

Síntese e caracterização de nanopartículas de CuO dopadas com Fe: Eficiência catalítica na degradação do corante cristal violeta e exploração de propriedades elétricas

Resumo

Nos últimos tempos, a poluição ambiental tornou-se uma questão premente. Diferentes métodos foram desenvolvidos para separar materiais perigosos de corpos de H_2O. Dentre essas técnicas, a fotocatálise emergiu como um método avançado e de baixo custo. No entanto, encontrar um fotocatalisador potente tem sido um tema

de considerável pesquisa. Em nosso estudo, preparamos CuO a partir de acetato de cobre por meio de tratamento hidrotérmico em autoclave a 170 °C por 14 horas. Introduzimos várias quantidades de Fe adicionando a mistura $FeSO_4$ ao Cu $(CH_3COO)_2$, seguindo o método idêntico ao da preparação de CuO. O precipitado resultante foi limpo com H_2O deionizada e seco a 100 °C. A substância preparada foi então aquecida a 450 °C em mufla por 1 hora. Caracterizamos a fabricação de fotocatalisadores utilizando diversas técnicas como Ultravioleta (UV), FT-IR, SEM, EDX e XRD. Nossa análise do espectro ultravioleta (UV) nos ajudou a reconhecer a análise espectroscópica de adsorção de CuO dopado e não dopado com várias proporções de Ferro. A análise espectroscópica FTIR nos ajudou a identificar grupos funcionais em NPs de óxido de Cobre. Nosso estudo de XRD mostrou a composição monoclínica de nanopartículas de óxido de cobre. A imagem SEM sugeriu que os NPs existem em forma esférica. Estudamos a atividade catalítica de NPs sintetizados em relação à degradação do corante violeta cristal (CV) abaixo de um raio direto de irradiação de luz. Nossos resultados mostraram que a produtividade da degradação, ao contrário do corante CV, foi de cerca de 93,52% em 180 min. Esta pesquisa é de grande importância na busca por soluções eficazes e sustentáveis para os problemas ambientais. O exame das propriedades elétricas destacou os aspectos promissores do CuO dopado com Fe, particularmente com 6% de dopagem. Esta variante demonstrou parâmetros dielétricos superiores, menor perda tangente, comportamento de impedância semelhante ao semicondutor e melhor condutividade elétrica, enfatizando seu potencial para aplicações em domínios elétricos e de armazenamento de energia.

Palavras-chave: método hidrotérmico, degradação fotocatalítica, corante violeta cristal.

1. Introduction

Copper oxide (CuO) is a semiconductor with a mono-clinic shape and many exciting properties, such as antimicrobic activities, high strength, and very good thermal conductivity. It is a p-type semiconductor having an energy gap of 1.2-1.9 eve. It is a black transition metal oxide with a host of intriguing features, including high thermal conductivity, photovoltaic capabilities, stability, and antibacterial activity. Owing to these characteristics, CuO has been thoroughly studied for a variety of possible uses, including gas sensors, field emitters, electrochemical cells, magnetic storage gadgets, and catalysis (Aparna et al., 2012; Ahamed et al., 2014, Saeed et al., 2024).

The most recent research suggests that differentiating the response of invisible surroundings with an oil and H_2O compound solvent as a medium could produce nanoparticles with varied sizes and shapes. Transition metal oxides are a necessary family of semiconductors used in electronics, catalysis, solar energy conversion, and magnetic storage media (Jiang et al., 1998; Rajamohan et al., 2023; Bakhtiar et al., 2024; Liu et al., 2024). Because of their effectiveness as tiny fluids in energy transfer applications, CuO NPs are one of the more intriguing transition metal oxides.

For instance, it has been noted that adding 4% CuO increases water's thermal conductivity by 20%. CuO is a small bandage semiconducting compound that finds usage in photothermal and photoconductive applications (Agarwal et al., 2016; Attiya et al., 2023; Naz et al., 2023; Muhammad et al., 2024). It can be utilized in a broad range of fields, such as photodetectors, batteries, supercapacitors, magnetic recording devices, and catalysis, among many others. Scientists are now motivated to manipulate its size and shape for optimal performance because of these characteristics (Ibupoto et al., 2018; Xu et al., 2020; Zhao et al., 2021). Effective biotic chemicals called copper compounds are frequently utilized in pesticide formulations and medical applications (Naika et al., 2015).

Accordingly, the synthesis of copper oxide nanoparticles (NPs) becomes imperative. Cu^+, Cu^{2+}, and Cu^{3+} are the three oxidation states that can occur in copper (Cu), and metal oxide nanoparticles (NPs) can be doped with both kinds of electrons and holes (Khmissi et al., 2016; Nazir et al., 2020; Ali et al. 2024). The electrical configuration of the host material (CuO) can be modified by carefully doping transition metal ions into it, which improves the conductivity and physical characteristics of the resulting synthetic nanoparticles (Bayansal et al., 2014; Balkrishna et al., 2021; Pervaiz et al., 2023). In comparison to single-element doping, co-doping (2 types of atoms) into semi-conductor oxides has attracted a lot of attention because it produces enhanced photocatalytic activity and a unique character (Viruthagiri et al., 2014; Khan et al., 2023; Ali et al., 2024).

Using the microwave approach, several research publications have shown how Ni doping affects the optical characteristics of pure CuO nanostructures (Thakur; Kumar, 2018; Zada et al., 2018; Zada et al., 2020; Shaheen et al., 2024). The physical and chemical characteristics of copper oxide nanoparticles make them intriguing from a technology standpoint. Intense heat superconductors, cells, gas detectors, catalysis, solar power conversion, and other applications can all benefit from their use.

Degradation of organic dyes using pure metallic nanoparticles is a popular area of research nowadays. Doping, on the other hand, modifies the electrical structures of native semiconductors to introduce flaws into their flawless crystal lattice and increase photocatalyst activity. These kinds of defects can capture holes or electrons produced during the photoexcitation process. Defect sites, like vacancies, also have an important role in enhancing the catalytic activation of strong bonds, which helps kinetic processes. Additionally, doping may cause the photocatalyst to produce more charge carriers, which could cause the bandage to change in size. To change photocatalytic activity in the direction of a substrate, doping can therefore change light adsorption, restrict re-combination through trap sites, and move Visual Basic (VB) or Citizens' Band (CB) locations (Xu et al., 2019; Sinha; De, 2020; Madani et al., 2021).

Other names for crystal violet (CV) include methyl violet 10B, crystal violet, and gentian violet 3. N-[4-[bis[4-(dimethyl amino)phenyl]methylene]-2 is its IUPAC name. methylene cyclohexadiene-1-ylide -2,5-N-methylmethanaminium chloride is a member of the triphenylmethane colorant class, with the molecular formula $C_{25}H_{30}N_3Cl$ and chemical weight 407.98. The greatest absorption wavelength is between 589 and 594 nanometers. Crystal violet is employed as a pH gauge, transitioning from yellow to violet at a pH of 1.6. It is utilized as an antibiotic factor in the pharmaceutics field and is the active element of Gram's stain. Both humans and creatures can use the colorant for outer skin disinfection. It is frequently utilized in paints and printing ink, as well as a purple colorant for fabrics like cotton and silk (Mittal et al., 2010; Hu et al., 2023; Khan et al., 2024).

It is widely employed in the food sector, veterinary medications, biological stains, commercial fabric dyeing, and leather processing. An overabundance of CV colorant in the human body can lead to tetraplegia, elevated heart rate, irritated eyes, and long-lived harm to the clear mucosa surrounding the eyes. Thus, it's critical to detach CV colorant from hazardous effluent. The literature has descriptions of several methods for decontaminating crystal violet color. These consist of coagulation, membrane-filtration, absorption, enhanced oxidation, biological therapy, electrolysis, and photocatalytic degradation (Hu et al., 2020; Abdelrahman et al., 2023; Muhiuddin et al., 2023).

A common technique for producing nanomaterial using a solution-based reaction strategy is hydrothermal synthesis. It is possible to do this operation at a variety of temperatures, from very hot to room temperature. Depending on the air pressure of the principal element in the reaction, either high high-pressure or low-pressure situation can be used to edit the form of the resultant nanomaterial. This procedure has been successfully utilized to produce a wide variety of tiny materials. Compared to other techniques, hydrothermal synthesis has a quantity of benefits. It may be used to create high vapor-pressure nanoparticles with little material loss as well as unstable nanomaterial at high temperatures. Chemical processes in the liquid phase or multiphase can be used to precisely control the composition of the nanomaterial. During the hydrothermal reaction, nucleation and grain growth mechanisms regulate the size of the particles. The temperature regulates their production rate while holding other factors constant (Liu et al., 2014; Darr et al., 2017; Yang; Park, 2019).

A thorough analysis of the publications that have already been published has revealed that no research has been done to date to ascertain the photocatalytic degradation of CV dye and electrical characteristics utilizing Fe-doped CuO NPs that are hydrothermally produced. In this context, NPs of copper oxide doped with iron were successfully synthesized via hydrothermal technique, and the structural, photocatalytic, and chemical stability were subsequently studied in the present research work.

2. Materials and Methods

2.1 Chemicals and reagents

All the chemicals and reagents utilized in the synthesis of CuO nanoparticles are of analytical grade. The Copper (II)-acetate-1-hydrate ($C_4H_6CuO_4.H_2O$) is purchased from Sigma-Aldrich laborchemikalien GMBH, Iron Sulfate heptahydrate ($FeSO_4.7H_2O$) is purchased from Polifar group, China, Sodium hydroxide (NaOH) were obtained from Sigma-Aldrich company, Germany, Crystal Violet colorant and Ethanol were obtain from Daejung chemicals, S. Korea some of the appreciable substance that is being used in the method of this hypothetical effort, all over the complete experimental efforts, mineral water is utilized.

2.2 Synthesis of CuO and Fe-doped CuO nanoparticles

The hydrothermal method was employed to synthesize pure CuO NPs (C1) and various Fe-doped nanoparticles (C2, C2, C3, C4, and C5). In this process, 5 g of cupric acetate was dissolved in 100ml of distilled water. Simultaneously iron sulfate was added to the mixture following the proportions outlined in (Table 1). The

resulting solution was stirred, and NaOH was then added. To maintain a pH of 10, Sodium hydroxide (NaOH) was added drop by drop to achieve a homogeneous solution leading to the formation of a particular precipitate. Subsequently, the homogeneous mixture was transformed into a stainless-steel Teflon autoclave and put through to a heat of 170 °C for 14 hours. After completion, the stainless-steel autoclave was allowed to cool, and the contents were then cleaned and centrifuged to remove any unreacted components. The resulting precipitate was subjected to calcination at 450 ̊C. The scheme of the process is given in (Figure 1). The sample procedure is followed for the production of pure CuO NPs (C1).

Table 1. Required ingredients for the preparation of the sample.

Samples name	Nature of NPs	Cupric acetate	Iron sulfate
C1	Pure CuO NPs	5 g	0 g
C2	2% Fe-doped CuO NPs	5 g	0.1 g
C3	4% Fe-doped CuO NPs	5 g	0.2 g
C4	6% Fe-doped CuO NPs	5 g	0.3 g
C5	8% Fe-doped CuO NPs	5 g	0.4 g

Source: Authors, 2024.

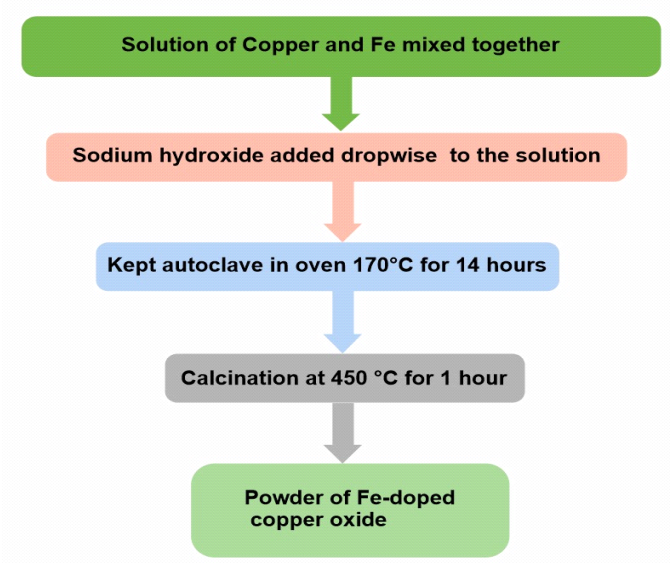

Figure 1. Schematic synthesis of Strontium oxide nanoparticles was conducted using a hydrothermal method. Source: Authors, 2024.

2.3 Photocatalytic degradation of CV dye

To perform the photocatalytic technique, a 100 W incandescent light bulb was utilized. A solution of 120 mL of CV with a concentration of 25 parts per million (ppm) was mixed with a dispersion of photo-catalysts. The solution was stirred at room temperature for 25 min without light, to establish an adsorption/desorption equilibrium. The mixture was then subjected to ionizing radiation therapy while being vigorously stirred. To ensure complete removal of all solid catalyst, a small amount of the solution (4-5 mL) was periodically removed and centrifuged. Finally, the effectiveness of the catalyst in dye adsorption and degradation was evaluated using a UV-visible spectrometer. The dye (%) elimination can be calculated using the provided formula.

$$\%\text{Degradation} = 100 \times (Co-Ct)/Co$$

Where: C_0 and C were initial and final concentrations after a particular time interval respectively.

2.4 Electrical properties

A precise impedance analyzer (MICROTEST, 6630, Taiwan) and 2401 Keithley Source Meter Unit (SMU) were used for measuring electrical conductivity. Both instruments provided accurate measurements of the electrical properties of the tested materials. The measured di-electric continuous as a duty of frequency.

2.5 Characterizations

Various characterization techniques were utilized to examine and recognize the characteristics of collected materials. UV-visible spectroscopy studied was managed utilizing a Shimadzu UV-1800 spectroscope, wavelength scale from 190-1100 nm, helping absorbance calculation. The Fourier-transform infrared spectroscopy (V. 640, USA) scale from 400 to 4000 cm^{-1} was utilized to examine association by establishment spectrum from a 0.09 g element. Photoluminescence (PL) analysis, accomplished at Abdul Wail Khan University Mandan, is involved in assessing substance clarity with a spectral scale of 230 to 1000 nm and a nontoxic procedure. X-ray diffraction diffract-meter (D-2 Passer, Barker, Denver, CO, USA) was utilized by employing 20 degrees per minute, and a Cu kα irradiation source was utilized, giving under-standings into the crystalline shape of the sample. The structure analysis of collected material was collected through a scanning electron microscope (SEM) (model, JSM5910, JEOL. Kyoto, Japan) with an increasing voltage of 30 Kv was utilized to search the outside and structure of the collected materials.

3. Results and Discussion

This study utilized various pathways to regulate the optic, structural, and key features of un-doped and Fe-doped CuO NPs. Measurement of the photo catalytic degradation of photocatalysis was performed using valuable crystal violet colorant below light irradiation.

3.1 Ultra-violet visible spectrometry

The UV-*Vis* Spectroscopy of the sample is shown in (Figure 2). The light absorption of the samples shows that all the samples absorb a major portion of light in the visible light range. The absorption ranges start roughly at 550 nm and increase as the wavelength increases. After the introduction of the iron in the parent CuO nanoparticles, the light absorption is further improved. This increase in light absorption plays a vital role in the photocatalytic process for pollutant degradation below the stipulated condition.

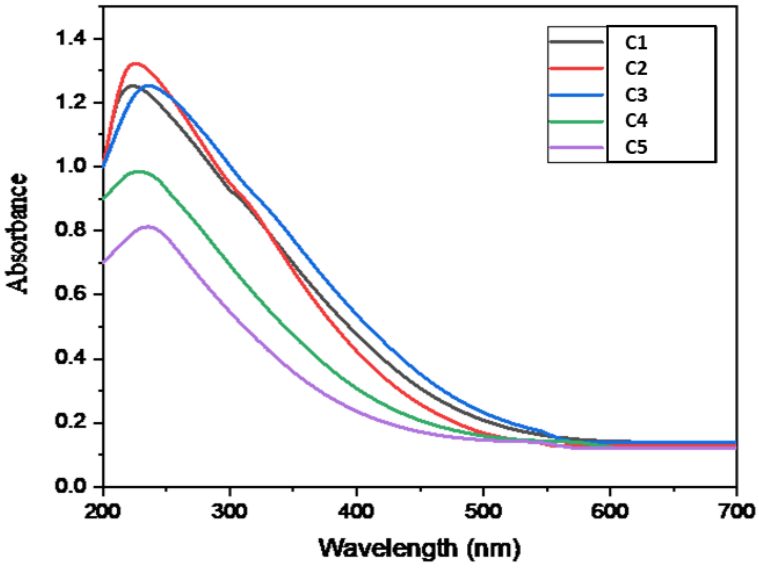

Figure 2. UV-visible spectroscopy of pure copper oxide and Fe-doped CuO NPs. Source: Authors, 2024.

3.2 Fourier transform infrared (FTIR) spectrometry

The Fourier-transform-infrared (FTIR) spectroscopy is a technique used to confirm the presence of molecular functional groups. The Fourier-transform-infrared (FTIR) scale was at 400 cm^{-1} to 4000 cm^{-1} and the result is shown in (Figure 3), the high peak at about 3300 cm^{-1} is caused by the absorbed H_2O molecules. This as it may be because of H_2O absorbed on the outer side of Cu nanoparticles. The two infrared adsorption peaks explicate the vibrational way of Cu nanoparticles on the scale of 500-800 cm^{-1}. Peaks between 400 and 600 cm^{-1}, such as 608, 480, and 450 cm^{-1}, are assigned to CuO species and confirm the presence of copper oxide. The peak at 580 cm^{1} could be the presence Fe-O stretching of in the C4 sample. (Khan et al., 2023).

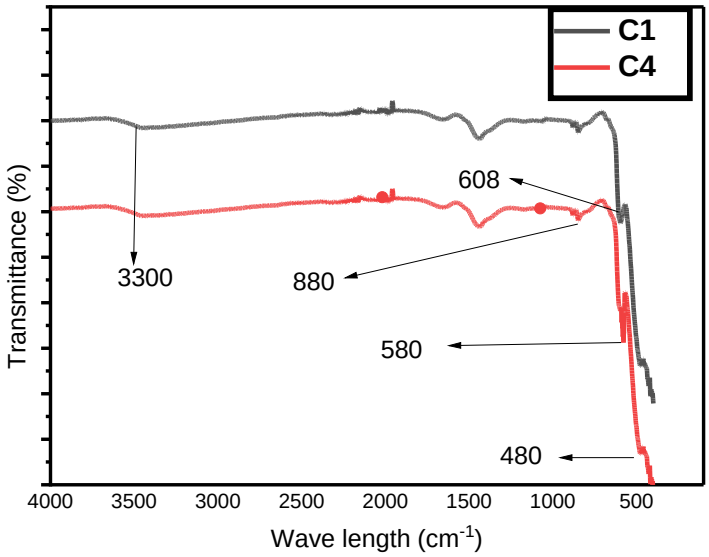

Figure 3. FTIR Spectra of synthesized C1 and C4 samples. Source: Authors, 2024.

3.3 X-ray diffraction analysis

X-ray diffraction analysis (XRD) is a highly effective way to note out about crystalline materials. It is a one-phase, crystalline, and mono-clinic shape of copper oxide nanoparticles. The X-ray diffraction analysis (XRD) detail from our sample is shown in (Figure 4). The dispersion peak at 2-theta = 32.46°, 35.46°, 38.65°, 48.68°, 53.37°, and 58.25° are compared to the crystal planes (110), (022), (111), (-202), (020), and (202) respectively.

X-ray diffraction analysis (XRD) shows that the compound is not one phase, and some more peaks are obtained due to an incomplete reaction. It is shown in the return plane at (110), (022), (111), (-202), (020), and (202) in the design, which can be connected to the monoclinic periods. Also, no emission peaks attached to Cu and other hazards are obtained in these patterns (Jabli, 2023; Yildirimcan, 2023; Mohanapandian et al., 2024).

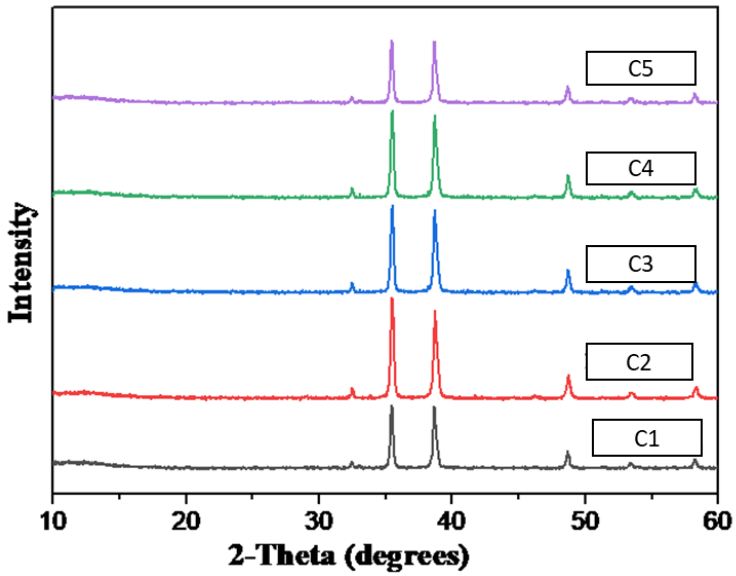

Figure 4. XRD pattern of C1, C2, C3, C4, and C5 samples. Source: Authors, 2024.

3.4 Energy dispersive X-ray (EDX) analysis

Because of its high reactivity, energy-dispersive X-ray is highly utilized in the identification of components. Observations of the synthesized nanoparticles using EDX were carried out on the energy scale of 0 to 20 KV. Figure 5 shows an energy-dispersive X-ray of 6% iron-doped copper oxide NPs. The figure shown that Cu and O both have large level peaks, while C have sharp-edged peak. It is highly pure that the sample involves all of the necessary components, which is evidence of the large purity of the sample. In addition, Cu and O are present in the sample 6% Fe-doped Cu NPs in essential amount, copper is present in a great amount which is 92.72 percent, but the amount of doped iron is almost 2.24 percent (as shown in Table 2). The remaining 5.04% is carbon.

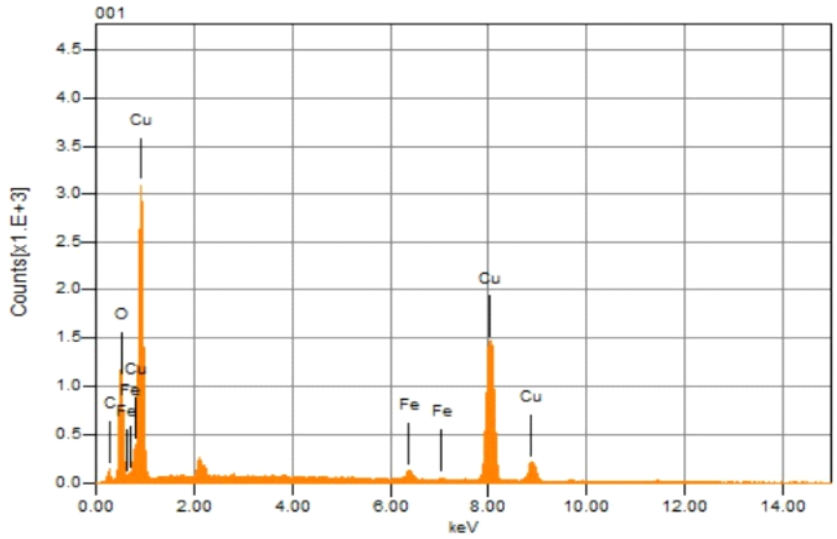

Formula	mass%	Atom%	Sigma	Net	K ratio	Line
C	5.04	15.79	0.02	2980	0.0004768	K
O	15.74	37.07	0.06	29894	0.0218571	K
Fe	2.24	1.51	0.05	6664	0.0050242	K
Cu	76.98	45.63	0.29	116559	0.1446562	K
Total	100.00	100.00				

Figure 5. EDX of C4 sample. Source: Authors, 2024.

3.5 Scanning electron microscopic (SEM) analysis

By applying microscopic investigation and reaction, the length of prepared un-doped and iron-doped Cu nanoparticles were acknowledged. As shown in Figure 6, from the SEM pictures of Cu nanoparticles, it seemed that all molecules of copper oxide are curved and continuous crystalline structures. There is a larger tendency for collection. The SEM images up-holds the evolution of the systematic polyhedron structure of the copper oxide nanoparticles. The evolution of the extremely press-down spherical pattern is noticed. In some regions, large nanoparticles are covered by small nanoparticles. Similar SEM images of Fe-doped copper oxide NPs were followed and detailed. These SEM pictures also recommend the small agglomeration of a tiny structure. However, a Fe-doped small composite shows rectangular agglomeration of smooth surfaces.

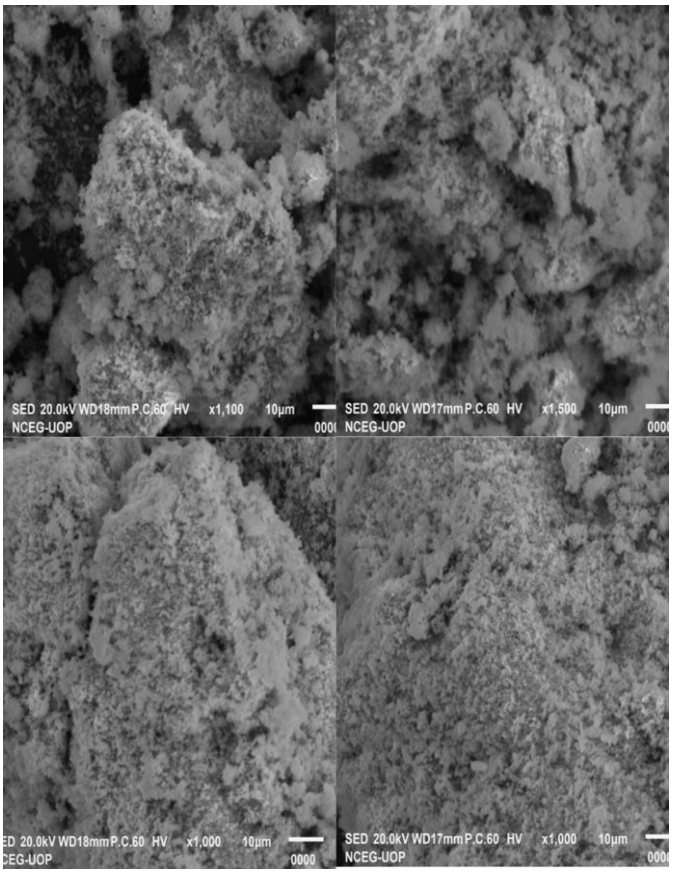

Figure 6. SEM images of C4. Source: Authors, 2024.

3.6 Photocatalytic degradation

The UV-visible adsorption scale of Crystal violet in the liquor shape is shown in (Figure 4.6) when the substance was uncovered to light at various periods from 0 to 180 min. The solutions hold for 30 min without light to achieve equilibrium between the absorption and desorption of the dye pieces. Illuminating the suspension with visible light from a 100 W incandescent lamp was picked at an away of 7 cm from the substance that was being explored. A piece of 10 mL was gathered at a time interval of 30 min in one of the reaction mixtures that were being upset regularly.

From that point onward, the mixture was heated for 5 min at a speed of 3000 rpm, and the outcome is shown in (Figure 7), As per the discovery, the adsorption of the crystal violet at 590 nm regularly reduces as the light time passes from 0 to 180 min. This process is noted all over the study. This recommends that the light-degradation of CV is time-relevant. In view of the results, clearly, all the photo-catalysts exhibited display extraordinary photo-catalytic motion as opposed to CV in the liquid intermediate. In the current analysis, the photo-catalytic degradation of CV in the liquid median is expected to photo-catalyst deposit. For 90, 120, 150, and 180 min of radiation, the degradation power of Crystal Violet seemed as much highly in the case of 8% Fe-doped copper

oxide (83.21%), 6% Fe-doped (86.08%), 4% Fe-doped (93.52%), 2% Fe-doped (88.11%), and un-doped copper oxide (85.23%). Figure 8 shows the degraded samples over different periods.

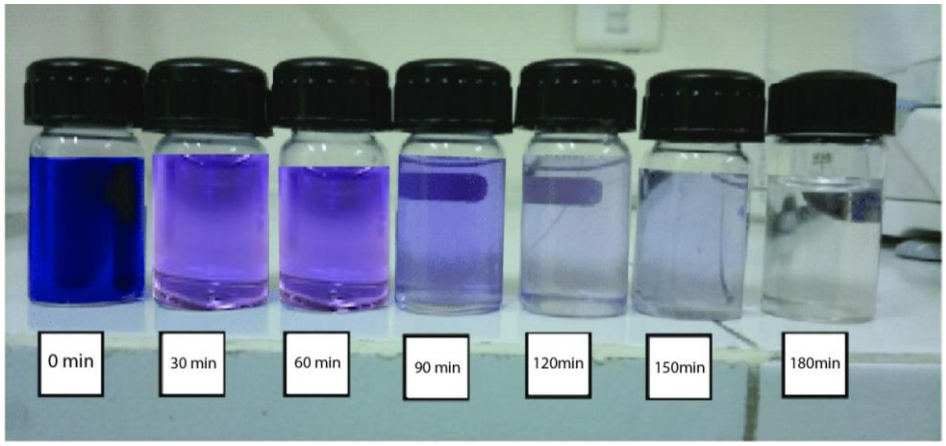

Figure 7. Treated and untreated CV dye solution of our experiment over various intervals. Source: Authors, 2024.

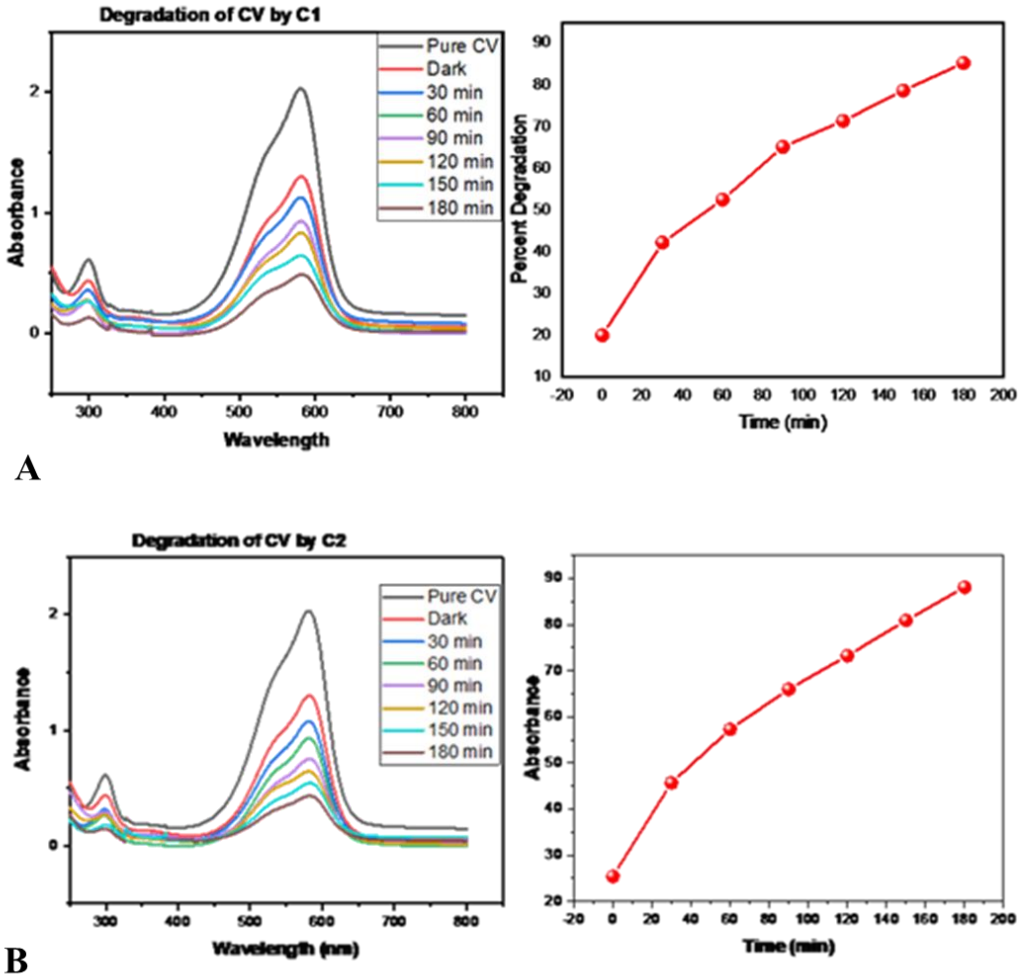

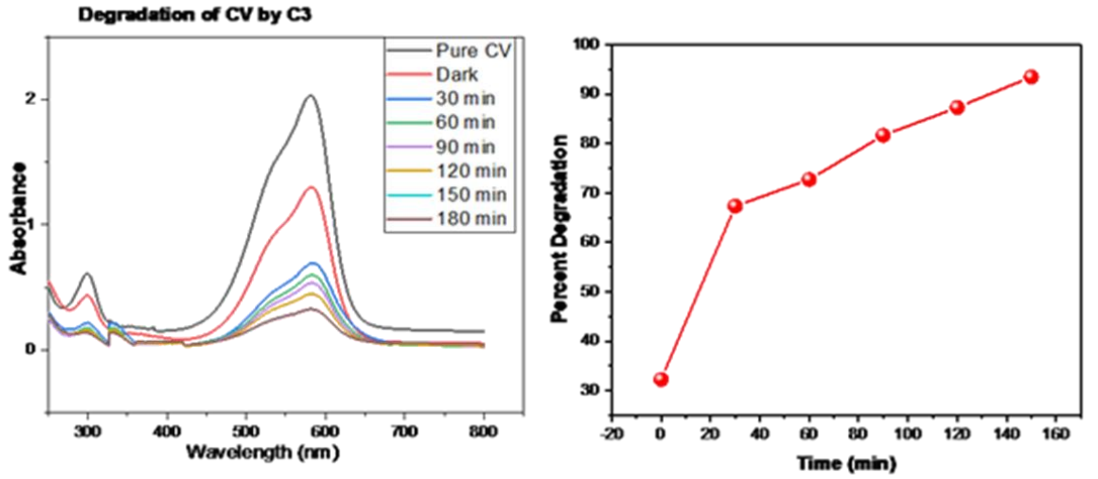

C

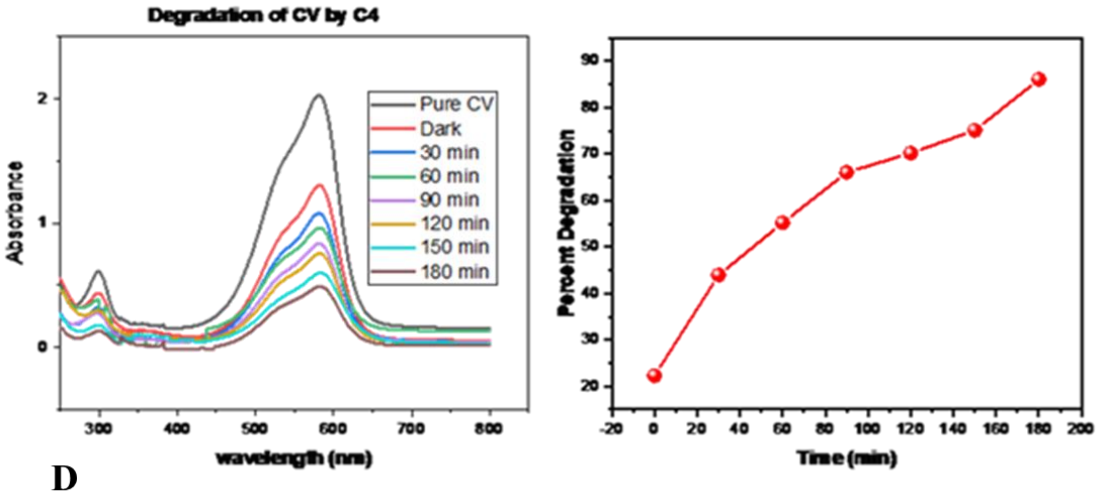

D

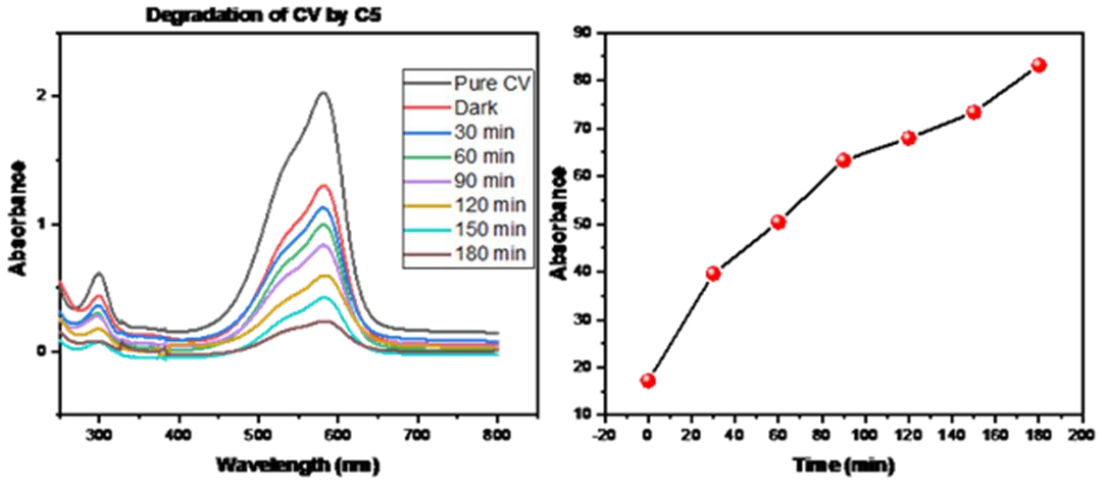

E

Figure 8. % photo-catalytic degradation of CV dye: **A**) % photo-catalytic degradation of CV dye by C1. **B)** % photo-catalytic degradation of CV dye by C2. **C)** % photo-catalytic degradation of CV dye by C3. **D)** % photo-catalytic degradation of CV dye by C4. **E)** % photo-catalytic degradation of CV dye by C5. Source: Authors, 2024.

Table 2. % photocatalytic degradation of CV dye by C1, C2, C3, and C4.

Time (min)	Percent Degradation				
	Pure CuO	2% Fe-CuO	4% Fe-CuO	6% Fe-CuO	8% Fe-CuO
0	20.01	25.42	32.23	22.29	17.25
30	42.22	45.67	67.34	43.98	39.6
60	52.52	57.28	72.72	55.23	50.4
90	65.16	65.96	81.69	66.05	63.31
120	71.37	73.24	87.34	70.22	67.96
150	78.65	80.89	93.52	75.12	73.37
180	85.23	88.11	-------	86.08	83.21

Source: Authors, 2024.

3.7 Electrical properties

The examination of dielectrics can aid in comprehending the influence of frequency on the conductive behavior of materials (Nano and microstructure) (Kao, 2004). They are valuable for closely scrutinizing the electrical properties of interfaces between grains within materials (Greuter et al., 1990; Lu et al., 2004; Guo; Waser, 2006). Dielectric characteristics describe how materials behave when exposed to an electric field (Martinez-Vega, 2013). The primary sources of materials are derived from various forms of polarization, such as electronic (Ishai et al., 2013), ionic (Maier, 2023), dipolar (Quan et al., 2017), and space charge (Lewiner; Insulation, 2010).

The most significant impact on polycrystalline materials is the polarization of electrons which stands out in the light spectrum (Moore; Smart, 2020). Dielectric parameters, including the dielectric constant (εr) and di-electric loss (tanδ), outline the essential electrical traits of CuO nanoparticles. Understanding how these variables fluctuate with varying frequencies provides insight into the electrical mechanisms occurring in CuO nanoparticles. We closely examined these factors to grasp the electrical properties of CuO nanoparticles.

From Figure 9**,** we can see that with an enhancement in frequency, the dielectric constant reduces, as the charge carriers become immobilized in diverse locations and orientations without alternating current. In the presence of an electric field, a charged particle can travel from one location to another, resulting in a change in the direction of an electric dipole (Oruç; Altındal, 2017).

This shows that the complex dielectric constant fluctuates depending on frequency and illustrates the amount of energy that a material can retain as polarization and the amount of energy that is dissipated (Schrödle et al., 2007). From Figure 1, with an enhancement in the doping concentration of iron in CuO its dielectric constant increases which means that the increase in the doping concentrations increased its energy storage ability. From Figure 1, we can see that the C4 exhibits higher storage ability than the rest of all.

The charge carrier is capable of relaxing by employing the dielectric loss mechanism. The loss tangent (tan) assesses the energy loss in comparison to the energy maintained in a periodic field. One can calculate it by dividing the energy loss by the energy stored and is given by,

$$tan\delta = \frac{\varepsilon''}{\varepsilon'} \quad (1)$$

Where: ε' and ε'' represent the actual and unreal pieces of the dielectric constant.

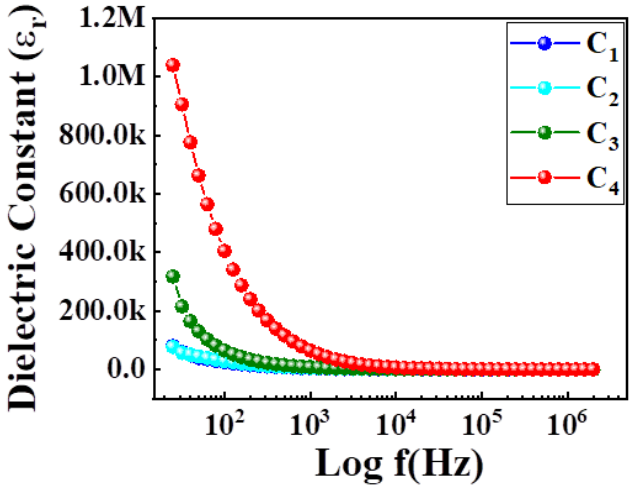

Figure 9. Shows various nanoparticles' dielectric constant as a function of frequency. Source: Authors, 2024.

Figure 10 represents the variation of frequency-dependent tan of copper oxide and iron-doped copper oxide nanoparticles at room temperature. As the frequency increases, the tangent loss increases at lower frequencies and a reverse trend occurs this is the increase in dielectric loss at higher frequencies. The increase in loss tangent is due to the dominance of the active part over the reactive part.

The reduce in tan can be assign to the separate results of the Ohm part and the reactive component, with the latter growing as the frequency rises (Bolivar et al., 2003). Looking at (Figure 2) indicates that C4 dissipates less energy than C1, C2, and C3 samples which means their ability to store energy increases, and the 6% doped exhibits the lowest energy loss.

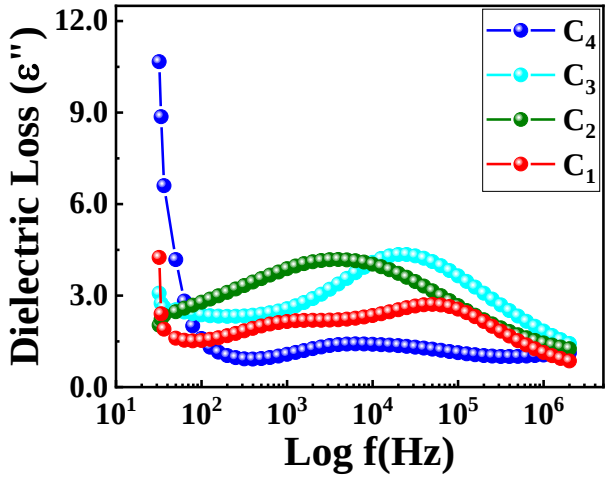

Figure 10. Shows various nanoparticles' tangent loss (tan) as a function of frequency. Source: Authors, 2024.

The pattern of the impedance as a work of frequency shows the same linear behavior at high frequency while the value impedance starts to decrease when frequency gradually increases. This implies that the impedance in the frequency domain shows the behavior of semiconductor. In the domain of frequency, the impedance suggests that the CuO is less effective at blocking electric charge, allowing it to be released.

With the addition of Fe doping to CuO nanoparticles, we can see the initial values at smaller frequencies and the final values at larger frequencies decrease. From Figure 3, the 6% Fe-doped CuO nanoparticles exhibit low resistivity which shows that the impedance decreases with the increase in doping concentrations. The findings demonstrate that as the frequency increases, so does the flow of electricity, as seen in (Figure 11)**.** This occurs due

to the discharge of the accumulated space charge.

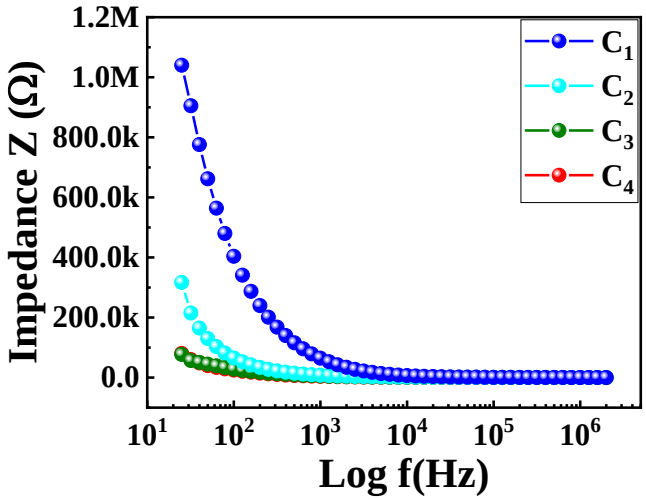

Figure 11. Shows the impedance spectroscopic behavior of prepared samples of Fe-doped CuO nanoparticles as a function of frequency. Source: Authors, 2024.

Figure 12 illustrates the variation of σ'_{ac} with increasing frequency on a logarithmic scale. The analysis of electrical conductivity (σ'_{ac}) on a logarithmic scale allowed us to investigate the flow of electricity at various frequencies. The correlated barrier hopping (CBH) model provides insights into interpreting our test findings (Jonscher, 1972). The movement of carriers in this model is a result of the barriers that exist between their respective locations. Figure 12 indicates a direct correlation between the total conductivity and increasing frequency. The conductivity of electricity is very good at higher frequencies.

Two distinct methods control the movement of particles as they leap from one location to another in a small piece of copper oxide, dictating how electricity flows through it (Sayer et al., 1978). Inter well hopping is the name utilized to express the motion of electricity from one hole to another within a material. In the second scenario, electrons move between holes within a defect potential well through a process known as intra-well hopping (Koshy et al., 2015). Figure 4 illustrates that variances in conductivity exhibit various trends. There are two parts: one for low frequencies and one for high frequencies.

The plateau region experiences a lower applied field frequency compared to the hopping frequency, which is when the pattern changes its slope. The conductance spectrum shows minimal variation at lower frequencies. At low frequencies, the conductance spectrum remains stable as the electric charge moves randomly. With an increase in AC frequency, there is also an increase in conductivity (Sati et al., 2014). As the frequency increases, more defects appear in the localized states, leading to higher conductivity at higher frequencies. This indicates that conductivity results from the transfer of charges between two locations (Sagadevan; Priya, 2015). Figure 12 Increments in the doping concentration cause an increase in AC conductivity. From this, the 6% Fe-doped CuO is a suitable material for electrical and storage applications.

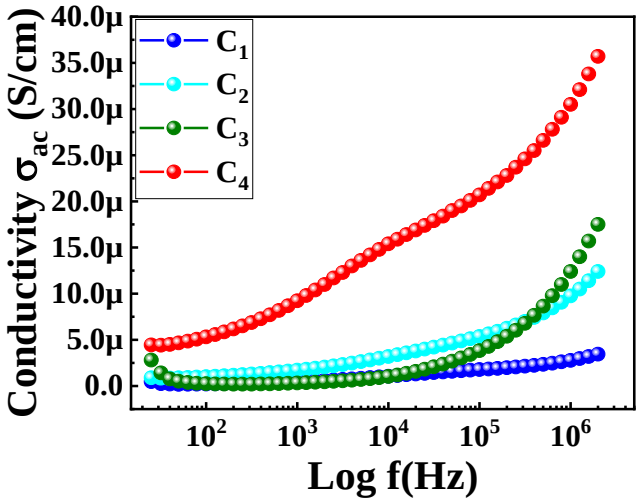

Figure 12. AC conductivity of various concentrations of C1, C2 C3, and C4. Source: Authors, 2024.

4. Conclusions

In conclusion, the combination of copper oxide and iron-doped Cu-O nanoparticles using an aqueous methodology resulted in well-defined particles with a size below 100 nm. Characterization through FTIR, UV-visible, XRD, SEM, and EDX established the mono-clinic crystalline shape of copper oxide nanoparticles (CuO) and the appearance of metal-oxygen bonds. The optic property of Fe-doped Cu-O was successfully investigated using a UV-visible spectrum. Beyond the structural and optical aspects, the study extended to the practical application of these materials in the detached crystal violet (CV) dye from H_2O. Copper oxide nanoparticles achieved an 85% removal rate, while Fe-doped CuO photocatalyst exhibited a significantly higher efficiency, degrading over 93% of the dye.

Furthermore, the examination of electrical properties highlighted the promising aspects of Fe-doped CuO, particularly at 6% doping. This variant demonstrated superior dielectric parameters, lower tangent loss, semiconductor-like impedance behavior, and enhanced electrical conductivity, emphasizing its potential for applications in electrical and energy storage domains.

In summary, the comprehensive investigation of synthesis, characterization, and application underscores the multifaceted potential of iron-doped copper oxide NPs. The combination of structural integrity, optical properties, and superior electrical characteristics positions these materials as promising candidates for diverse technological applications, including environmental remediation and advanced energy storage systems

5. Acknowledgments

The author is greatly acknowledging the Department of Chemistry, Abdul Wali Khan University Mardan, and Government Postgraduate College Nowshera, Khyber Pakhtunkhwa, Pakistan for providing experimental facilities.

6. Authors' Contributions

Bushra: conceptualization, methodology, and project oversight. Synthesis and characterization lead. Contributed significantly to catalytic efficacy analysis. *Muhammad Kashif*: key role in synthesis, characterization, and electrical property exploration. Contributed to manuscript drafting and revision. *Khairullah*: contributed to synthesis, characterization, and catalytic efficacy studies. Co-writer of the manuscript. *Azmat Ali Khan*: involved in synthesis, characterization, and electrical property exploration. Contributed to manuscript writing and revision. *Hao Sun*: collaborated on synthesis, characterization, and electrical property exploration. Contributed to manuscript drafting. *Jasim Kamal*: key role in catalytic efficacy studies. Contributed to synthesis, characterization, and manuscript drafting. *Muhammad Ishaq Ali Shah*: involved in the synthesis, characterization, and electrical property exploration. Contributed to manuscript drafting. *Shah Hussain*: expertise in synthesis, characterization, and catalytic efficacy studies. Contributed to manuscript drafting. *Jalal Amir*: crucial role in synthesis and characterization. Involved in electrical property exploration. Contributed to manuscript drafting. *Yousaf Jamal*: design, data exploration, Guidness, synthesis. *Taimoor Ahmad:* methodology, research design,

manuscript drifting.

7. Conflicts of Interest

No conflicts of interest.

8. Ethics Approval

Not applicable.

9. References

Abdelrahman, E. A., Algethami, F. K., AlSalem, H. S., Binkadem, M. S., Saad, F. A., El-Sayyad, G. S., Raza, N., & ur Rehman, K. (2023). Facile synthesis and characterization of novel nanostructures for the efficient disposal of crystal violet dye from aqueous media. *Inorganics*, 11(8), 339. https://doi.org/10.3390/inorganics11080339

Agarwal, R., Verma, K., Agrawal, N. K., Duchaniya, R. K., & Singh, R. (2016). Synthesis, characterization, thermal conductivity and sensitivity of CuO nanofluids. *Applied Thermal Engineering*, 102, 1024-1036. https://doi.org/10.1016/j.applthermaleng.2016.04.051

Ahamed, M., Alhadlaq, H. A., Khan, M A. M., Karuppiah, P., & Al-Dhabi, N. A. (2014). Synthesis, characterization, and antimicrobial activity of copper oxide nanoparticles. *Journal of Nanomaterials*, 2014, 17-17. http://dx.doi.org/10.1155/2014/637858

Ali, S., Ali, S., Khan, I., Zahid, M., Ismail, P. M., Ismail, A., Zada, A., Ullah, R., Hayat, S., Ali, H., Kamal, M. R., Alibrahim, K. A., Bououdina, M., Bakhtiar, S. H., Wu, X., Wang, Q., Raziq, F., & Qiao, L. (2024). Molecular modulation of interfaces in a Z-scheme van der Waals heterojunction for highly efficient photocatalytic CO_2 reduction. *Journal of Colloid and Interface Science*, 663, 31-42. https://doi.org/10.1016/j.jcis.2024.02.081

Ali, S., Ismail, P. M., Khan, M., Dang, A., Ali, S., Zada, A., Raziq, F., Khan, I., Khan, M. S., Ateeq, M., Khan, W., Bakhtiar, S. H., Ali, H., Wu, X., Shah, M. I., Vinu, A., Yi, J., Xia, P., & Qiao, L. (2024). Charge transfer in TiO 2-based photocatalysis: fundamental mechanisms to material strategies. *Nanoscale*, 9(16), 4352-4377. https://pubs.rsc.org/en/content/articlelanding/2024/nr/d3nr04534j/unauth

Aparna, Y., Rao, K. V. E., & Subbarao, P. S. (2012). Synthesis and characterization of CuO nano particles by novel sol-gel method. *In*: Proceedings of the 2nd International Conference on Environment Science and Biotechnology, IACSIT Press Singapore, 48, 156-160 p. https://doi.org/10.7763/IPCBEE

Attiya, H. G., Fendi, W. J., Al-Dulaimy, Z. A., Farooq, A., & Mohammed, A. M. (2023). Characterization synthesis of Copper oxide. Nanoparticles application. A review. *Journal of Pharmaceutical Negative Results*, 14(2), 250-256. https://doi.org/10.47750/pnr.2023.14.S02.32

Balkrishna, A., Arya, V., Rohela, A., Kumar, A., Verma, R., Kumar, D., Nepovimova, E., Kuca, K., Thakur, N., Thakur, N., & Kumar, P. (2021). Nanotechnology interventions in the management of COVID-19: prevention, diagnosis and virus-like particle vaccines. *Vaccines*, 9(10), 1129. https://doi.org/10.3390/vaccines9101129

Bayansal, F., Taşköprü, T., Şahin, B., & Çetinkara, H. A. (2014). Effect of cobalt doping on nanostructured CuO thin films. *Metallurgical and Materials Transactions A*, 45, 3670-3674. https://doi.org/10.1007/s11661-014-2306-1

Bolivar, P. H., Brucherseifer, M., Rivas, J. G., Gonzalo, R., Ederra, I., Reynolds, A. L., Holker, M., & Maagt, P.. (2003). Measurement of the dielectric constant and loss tangent of high dielectric-constant materials at terahertz frequencies. *IEEE - Transactions on Microwave Theory and Techniques*, 51(4), 1062-1066. https://doi.org/10.1109/TMTT.2003.809693

Darr, J. A., Zhang, J., Makwana, N. M., & Weng, X. (2017). Continuous hydrothermal synthesis of inorganic nanoparticles: applications and future directions. *Chemical Reviews*, 117(17), 11125-11238. https://doi.org/10.1021/acs.chemrev.6b00417

Greuter, F., & Blatter. (1990). Electrical properties of grain boundaries in polycrystalline compound semiconductors. *Semiconductor Science and Technology*, 5(2), 111. DOI 10.1088/0268-1242/5/2/001

Guo, X., & Waser, R. (2006). Electrical properties of the grain boundaries of oxygen ion conductors: acceptor-doped zirconia and ceria. *Progress in Materials Science*, 51(2), 151-210. https://doi.org/10.1016/j.pmatsci.2005.07.001

Hu, D., Song, T., Zada, A., Yan, R., Li, Z., Zhang, Z., Bian, J., Qu, Y., & Jing, L. (2023). Graphene oxide modulated dual S-scheme ultrathin heterojunctions with iron phthalocyanine and phase-mixed bismuth molybdate as wide visible-light catalysts. *Environmental Science: Nano*, 10(3), 922-932.

Hu, X., Yan, L., Wang, Y., Xu, M. (2020). Freeze-thaw as a route to build manageable polysaccharide cryogel for deep cleaning of crystal violet. *Chemical Engineering Journal*, 396, 125354. https://doi.org/10.1016/j.cej.2020.125354

Ibupoto, Z. H., Tahira, A., Raza, H., Ali, G., Khand, A. A., Jilani, N. S., Mallah, A. B., Yu, C., & Willander, M. (2018). Synthesis of heart/dumbbell-like CuO functional nanostructures for the development of uric acid biosensor. *Materials*, 11(8), 1378. https://doi.org/10.3390/ma11081378

Ishai, P. B., Talary, M. S., Caduff, A., Levy, E., & Feldman, Y. (2013). Electrode polarization in dielectric measurements: A review. *Measurement Science and Technology*, 24(10), 102001. DOI 10.1088/0957-0233/24/10/102001

Jabli, M. (2023). Preparation of alkali lignin extracted from ligno-cellulosic populus tremula fibers: Application to copper oxide nanoparticles synthesis, characterization, and methylene blue biosorption study. *International Journal of Biological Macromolecules*, 226, 956-964. https://doi.org/10.1016/j.ijbiomac.2022.12.097

Jonscher, A. K. (1972). Frequency-dependence of conductivity in hopping systems. *Journal of Non-Crystalline Solids*, 8-10, 293-315. https://doi.org/10.1016/0022-3093(72)90151-2

Kao, K. C. (2004). Dielectric phenomena in solids. With emphasis on physical concepts of eletronic processes. Elsevier Academic Press.

Khan, I., Liao, B., khan, S., Zada, A., Ali, S., Rizwan, M., Khan, A., Shah, M. I., & Alodhayb, A. (2023). Engineering selective CO_2 photoreduction by tailored interfacial design of P-modulated CuPc/B-C3N4 heterojunction for improved C_2H_4 selectivity. *Catalysis Science & Technology*.

Khan, M., Hussain, A., Saleh, M. T., Ibrahim, M., Attique, F., Sun, X., Unalan, H. E., Shafi, M., Khan, Y., Khan, I., Ragab, A. H., Hassan, A. A., Ali, R., Ali, Z., Khan, A. J., & Zada, A. (2024). Cutting-edge advancements in MXene-derived materials: Revolutionary electrocatalysts for hydrogen evolution and high-performance energy storage. *Coordination Chemistry Reviews*, 506, 215722. https://doi.org/10.1016/j.ccr.2024.215722

Khan, M., Khan, A. A., Parveen, A., Min, K., Yadav, V. K., Khan, A. U., & Alam, M. (2023). Mitigating the growth of plant pathogenic bacterium, fungi, and nematode by using plant-mediated synthesis of copper oxide nanoparticles (CuO NPs). *Green Chemistry Letters and Reviews*, 16(1), 2177520. https://doi.org/10.1080/17518253.2023.2177520

Khmissi, H., El Sayed, A. M., & Shaban, M. (2016). Structural, morphological, optical properties and wettability of spin-coated copper oxide; influences of film thickness, Ni, and (La, Ni) co-doping. *Journal of Materials Science*, 51, 5924-5938. https://doi.org/10.1007/s10853-016-9894-7

Koshy, J., Soosen, S. M., Chandran, A., & George, K. C. (2015). Correlated barrier hopping of CuO nanoparticles. *Journal of Semiconductors*, 36(12), 122003. DOI 10.1088/1674-4926/36/12/122003

Lewiner, J. (2010). Space charge and polarization in insulators: a long history with a promising future. *IEEE - Transactions on Dielectrics and Electrical Insulation*, 17(4), 1096-1105. https://ieeexplore.ieee.org/xpl/RecentIssue.jsp?punumber=94

Liu, N., Chen, X., Zhang, J., & Schwank, J. W. (2014). A review on TiO2-based nanotubes synthesized via hydrothermal method: Formation mechanism, structure modification, and photocatalytic applications. *Catalysis Today*, 225, 34-51. https://doi.org/10.1016/j.cattod.2013.10.090

Lu, L., Shen, Y., Chen, X., Qian, L., & Lu, K. (2004). Ultrahigh strength and high electrical conductivity in copper. *Science*, 304(5669), 422-426. https://doi.org/10.1126/science.1092905

Madani, S. S., Habibi-Yangjeh, A., Asadzadeh-Khaneghah, S., Chand, H., Krishnan, V., & Zada, A. (2021). Integration of $Bi_4O_5I_2$ nanoparticles with ZnO: impressive visible-light-induced systems for elimination of aqueous contaminants. *Journal of the Taiwan Institute of Chemical Engineers*, 119, 177-186. https://doi.org/10.1016/j.jtice.2021.01.020

Maier, J. (2023). Physical chemistry of ionic materials: Ions and electrons in solids. Second Edition, John Wiley & Sons.

Martinez-Vega, J. (2013). Dielectric materials for electrical engineering. ISTE, John Wiley & Sons.

Mittal, A.,Mittal J., Malviya, A., Kaur, D., & Gupta, V. K. (2010). Adsorption of hazardous dye crystal violet from wastewater by waste materials. *Journal of Colloid and Interface Science*, 343(2), 463-473. https://www.cabidigitallibrary.org/doi/full/10.5555/20103071066

Mohanapandian, K., Ponnarasan, V., & Thirupathy, J. (2024). An investigation on structural, dielectric and optical properties of pure and Fe-doped CuO nanoparticles for optoelectronic device applications. *Optical and Quantum Electronics*, 56(3), 347. https://doi.org/10.1007/s11082-023-05977-1

Moore, E. A., & Smart, L. E. (2020). Solid state chemistry and introduction. Chapter: Optical properties of solids. Solid State Chemistry, 5th Edition, 32 p.

Muhammad, P., Zada, A., Eashid, J., Hanif, S., Gao, H., Li, C., Li, Y., Fan, K., & Wang, Y. (2024). Defect engineering in nanocatalysts: From design and synthesis to applications. *Advanced Functional Materials*, 2314686. https://doi.org/10.1002/adfm.202314686

Muhiuddin, G., Bibi, I., Nazeer, Z., Majid, F., Kamal, S., Kausar, A., Raza, Q., Alwadai, N., Ezzine, S., & Iqbal, M. (2023). Synthesis of Ni doped barium hexaferrite by microemulsion route to enhance the visible light-driven photocatalytic degradation of crystal violet dye. *Ceramics International*, 49(3), 4342-4355. https://doi.org/10.1016/j.ceramint.2022.09.319

Naika, H. R., Lingaraju, K., Manjunath, K., Kumar, D., Nagaraju, G., Suresh, D., & Ngagabhushana, H. (2015). Green synthesis of CuO nanoparticles using *Gloriosa superba* L. extract and their antibacterial activity. *Journal of Taibah University for Science*, 9(1), 7-12. https://doi.org/10.1016/j.jtusci.2014.04.006

Naz, S., Gul, A., Zia, M., & Javed, R. (2023). Synthesis, biomedical applications, and toxicity of CuO nanoparticles. *Applied Microbiology and Biotechnology*, 107(4), 1039-1061. https://doi.org/10.1007/s00253-023-12364-z

Nazir, R., Khan, M., Riaz-ur-Rehman, Shujah, S., Khan, M., Ullah, M., Zada, A., Mahmood, N., & Ahmad, I. (2020). Adsorption of selected azo dyes from an aqueous solution by activated carbon derived from Monotheca buxifolia waste seeds. *Soil and Water Research*, 15(3), 166-172. https://www.cabidigitallibrary.org/doi/full/10.5555/20203445539

Oruç, Ç., & Altındal, A. (2017). Structural and dielectric properties of CuO nanoparticles. *Ceramics International*, 43(14), 10708-10714. https://doi.org/10.1016/j.ceramint.2017.05.006

Pervaiz, S., Shah, S. W. H., ul Wahab, Z., Farooq, M., Hallem, A., & Zada, A. (2023). Oil mediated polymer based green synthesis of calcium hydroxide nanoparticles and their application in bone conservation. *Zeitschrift für Physikalische Chemie*. https://doi.org/10.1515/zpch-2023-0452

Quan, B., Liang, X., Ji, G., Xheng, Y., Liu, W., Ma, J., Zhang, Y., Li, D., & Xu, G. (2017). Dielectric polarization in electromagnetic wave absorption: review and perspective. *Journal of Alloys and Compounds*, 728, 1065-1075. https://doi.org/10.1016/j.jallcom.2017.09.082

Saeed, F., Ahmad, M., Samia, Zada, A., Qi, D., & Wang, Y. (2024). Phosphorus-doped $CoFe_2O_4$ nanoparticles decorated nitrogen-doped graphene for efficient and stable electrocatalytic water splitting. *International Journal of Hydrogen Energy*, 59, 1196-1204. https://doi.org/10.1016/j.ijhydene.2024.01.035

Sagadevan, S., & Murugasen, P. (2015). Electrical properties of copper oxide nanoparticles. *Journal of Nano Research*, 30, 1-8. https://doi.org/10.4028/www.scientific.net/JNanoR.30.1

Sati, P. C., Arora, M., Chauhan S., Kumar, M., & Chhoker, S. (2014). Structural, magnetic, vibrational and impedance properties of Pr and Ti codoped $BiFeO_3$ multiferroic ceramics. *Ceramics International*, 40(6), 7805-7816. https://doi.org/10.1016/j.ceramint.2013.12.124

Sayer, M., Mansingh, A., Webb, J. B., & Noad, J. (1978). Long-range potential centres in disordered solids. *Journal of Physics C: Solid State Physiccs*, 11(2), 315. DOI 10.1088/0022-3719/11/2/016

Schrödle, S., Annat, G., MacFarlane, D. R., Forsyth, M., Buchner, R., & Hefter, G. (2007). "High frequency dielectric response of the ionic liquid N-methyl-N-ethylpyrrolidinium dicyanamide. *Australian Journal of Chemistry*, 60(1), 6-8. https://doi.org/10.1071/CH06251

Shaheen, S., Xu, S., Bian, J., Zada, A., Zhang, Z-Q., Qu, Y., & Jing, L-Q. (2024). Facile synthesis of hierarchical $NiO/NiFe_2O_4$ microsphere composite as efficient visible photocatalyst for 2, 4-DCP degradation. *Rare Metals*, 43, 1-9. https://doi.org/10.1007/s12598-023-02585-6

Sinha, I., & De, A. K. (2020). An overview of synthesis techniques for preparing doped photocatalysts. *Nano-Materials as Photocatalysts for Degradation of Environmental Pollutants*, 1-13, Chapter 1. https://doi.org/10.1016/B978-0-12-818598-8.00001-8

Thakur, N., & Kumar, J. (2018). Synthesis characterization and antibacterial study of co doped copper oxide nanoparticles. http://hdl.handle.net/10603/340612

Viruthagiri, G., Gopinathan, E., Shanmugam, N., & Gobi, R. (2014). Synthesis and characterization of ZrO_2–CuO co-doped ceria nanoparticles via chemical precipitation method. *Spectrochimica Acta Part A: Molecular and Biomolecular Spectroscopy*, 131, 556-563. https://doi.org/10.1016/j.saa.2014.04.117

Xu, B., Zada, A., Wang, G., & Qu, Y. (2019). Boosting the visible-light photoactivities of $BiVO_4$ nanoplates by Eu doping and coupling CeO_x nanoparticles for CO_2 reduction and organic oxidation. *Sustaibable Energy & Fuels*, 3(12), 3363-3369. https://pubs.rsc.org/en/content/articlelanding/2019/se/c9se00409b/unauth

Xu, M., Zada, A., Yan, R., Li, H., Sun, N., & Qu, Y. (2020). Ti_2O_3/TiO_2 heterophase junctions with enhanced charge separation and spatially separated active sites for photocatalytic CO_2 reduction. *Physical Chemistry Chemical Physics*, 22(8), 4526-4532. https://pubs.rsc.org/en/content/articlelanding/2020/cp/c9cp05147c/unauth

Yang, G., & Park, S-J. (2019). Conventional and microwave hydrothermal synthesis and application of functional materials: A review. *Materials*, 12(7), 1177. https://doi.org/10.3390/ma12071177

Yildirimcan, S. (2023). "Effect of ageing on electrical properties of Fe-doped CuO thin films deposited by spin coating technique. *Indian Journal of Physics*, 97(6), 1707-1716. https://doi.org/10.1007/s12648-022-02511-z

Zada, A., et al. (2020). Surface plasmon resonance excited electron induction greatly extends H_2 evolution and pollutant degradation activity of $g\text{-}C_3N_4$ under visible light irradiation. *Journal of the Chinese Chemical Society*, 67(6), 983-989. https://doi.org/10.1002/jccs.201900398

Zada, A., Qu, Y., Ali, S., Sun, N., Lu, H., Yan, R., Zhang, X., & Jing, L. (2018). Improved visible-light activities for degrading pollutants on $TiO_2/g\text{-}C_3N_4$ nanocomposites by decorating SPR Au nanoparticles and 2, 4-dichlorophenol decomposition path. *Journal of Hazardous Materials*, 342, 715-723. https://doi.org/10.1016/j.jhazmat.2017.09.005

Zhao, Y., Zada, A., Yang, Y., Pan, J., Wang, Y., Yan, Z., Xu, Z., & Qi, K. (2021). Photocatalytic removal of antibiotics on g-C3N4 using amorphous CuO as cocatalysts. *Frontiers in Chemistry*, 9, 797738. https://doi.org/10.3389/fchem.2021.797738

Funding

Not applicable.

Institutional Review Board Statement

Not applicable.

Informed Consent Statement

Not applicable.